

- Eriksson, P.S., Perfilieva, E., Björk-Eriksson, T., Alborn, A.-M., Nordborg, C., Peterson, D.A., Gage, F.H., 1998. Neurogenesis in the adult human hippocampus. *Nat. Med.* 4, 1313–1317.
- Espada, J., 2012. Non-catalytic functions of DNMT1. *Epigenetics* 7, 115–118.
- Espada, J., Peinado, H., Lopez-Serra, L., Setién, F., Lopez-Serra, P., Portela, A., Renart, J., Carrasco, E., Calvo, M., Juarranz, A., Cano, A., Esteller, M., 2011. Regulation of SNAIL1 and E-cadherin function by DNMT1 in a DNA methylation-independent context. *Nucleic Acids Res.* 39, 9194–9205.
- Fan, G., Beard, C., Chen, R.Z., Csankovszki, G., Sun, Y., Siniaia, M., Biniszkiwicz, D., Bates, B., Lee, P.P., Kuhn, R., Trumpp, A., Poon, C., Wilson, C.B., Jaenisch, R., 2001. DNA hypomethylation perturbs the function and survival of CNS neurons in postnatal animals. *J. Neurosci.* 21, 788–797.
- Fan, G., Martinowich, K., Chin, M.H., He, F., Fouse, S.D., Hutnick, L., Hattori, D., Ge, W., Shen, Y., Wu, H., ten Hoeve, J., Shuai, K., Sun, Y.E., 2005. DNA methylation controls the timing of astroglialogenesis through regulation of JAK–STAT signaling. *Development* 132, 3345–3356.
- Feng, J., Zhou, Y., Campbell, S.L., Le, T., Li, E., Sweatt, J.D., Silva, A.J., Fan, G., 2010. Dnmt1 and Dnmt3a maintain DNA methylation and regulate synaptic function in adult forebrain neurons. *Nat. Neurosci.* 13, 423–430.
- Gage, F.H., 2000. Mammalian neural stem cells. *Science* 287, 1433–1438.
- Georgia, S., Kanji, M., Bhushan, A., 2013. DNMT1 represses p53 to maintain progenitor cell survival during pancreatic organogenesis. *Genes Dev.* 27, 372–377.
- Hackam, A.S., Yassa, A.S., Singaraja, R., Metzler, M., Gutekunst, C.A., Gan, L., Warby, S., Wellington, C.L., Vaillancourt, J., Chen, N., Gervais, F.G., Raymond, L., Nicholson, D.W., Hayden, M.R., 2000. Huntingtin interacting protein 1 induces apoptosis via a novel caspase-dependent death effector domain. *J. Biol. Chem.* 275, 41299–41308.
- Hutnick, L.K., Golshani, P., Namihira, M., Xue, Z., Matyina, A., Yang, X.W., Silva, A.J., Schweizer, F.E., Fan, G., 2009. DNA hypomethylation restricted to the murine forebrain induces cortical degeneration and impairs postnatal neuronal maturation. *Hum. Mol. Genet.* 18, 2875–2888.
- Imayoshi, I., Ohtsuka, T., Metzger, D., Chambon, P., Kageyama, R., 2006. Temporal regulation of Cre recombinase activity in neural stem cells. *Genesis* 44, 233–238.
- Imayoshi, I., Sakamoto, M., Kageyama, R., 2011. Genetic methods to identify and manipulate newly born neurons in the adult brain. *Front. Neurosci.* 5, 64.
- Kempermann, G., Jessberger, S., Steiner, B., Kronenberg, G., 2004. Milestones of neuronal development in the adult hippocampus. *Trends Neurosci.* 27, 447–452.
- Kimura, H., Nakamura, T., Ogawa, T., Tanaka, S., Shiota, K., 2003. Transcription of mouse DNA methyltransferase 1 (Dnmt1) is regulated by both E2F-Rb-HDAC-dependent and -independent pathways. *Nucleic Acids Res.* 31, 3101–3113.
- Klose, R.J., Bird, A.P., 2006. Genomic DNA methylation: the mark and its mediators. *Trends Biochem. Sci.* 31, 89–97.
- Kriegstein, A., Alvarez-Buylla, A., 2009. The glial nature of embryonic and adult neural stem cells. *Annu. Rev. Neurosci.* 32, 149–184.
- Kronenberg, G., Reuter, K., Steiner, B., Brandt, M.D., Jessberger, S., Yamaguchi, M., Kempermann, G., 2003. Subpopulations of proliferating cells of the adult hippocampus respond differently to physiologic neurogenic stimuli. *J. Comp. Neurol.* 467, 455–463.
- Kuhn, H.G., Dickinson-Anson, H., Gage, F.H., 1996. Neurogenesis in the dentate gyrus of the adult rat: age-related decrease of neuronal progenitor proliferation. *J. Neurosci.* 16, 2027–2033.
- Lewis, A., Mitsuya, K., Umlauf, D., Smith, P., Dean, W., Walter, J., Higgins, M., Feil, R., Reik, W., 2004. Imprinting on distal chromosome 7 in the placenta involves repressive histone methylation independent of DNA methylation. *Nat. Genet.* 36, 1291–1295.
- Lois, C., Hong, E.J., Pease, S., Brown, E.J., Baltimore, D., 2002. Germline transmission and tissue-specific expression of transgenes delivered by lentiviral vectors. *Science* 295, 868–872.
- Lugert, S., Basak, O., Knuckles, P., Haussler, U., Fabel, K., Gotz, M., Haas, C.A., Kempermann, G., Taylor, V., Giachino, C., 2010. Quiescent and active hippocampal neural stem cells with distinct morphologies respond selectively to physiological and pathological stimuli and aging. *Cell Stem Cell* 6, 445–456.
- Ma, D.K., Marchetto, M.C., Guo, J.U., Ming, G.L., Gage, F.H., Song, H., 2010. Epigenetic choreographers of neurogenesis in the adult mammalian brain. *Nat. Neurosci.* 13, 1338–1344.
- McCabe, M.T., Davis, J.N., Day, M.L., 2005. Regulation of DNA methyltransferase 1 by the pRb/E2F1 pathway. *Cancer Res.* 65, 3624–3632.
- Meehan, R.R., 2003. DNA methylation in animal development. *Semin. Cell Dev. Biol.* 14, 53–65.
- Metzler, M., Gan, L., Wong, T.P., Liu, L., Helm, J., Liu, L., Georgiou, J., Wang, Y., Bissada, N., Cheng, K., Roder, J.C., Wang, Y.T., Hayden, M.R., 2007. NMDA receptor function and NMDA receptor-dependent phosphorylation of huntingtin is altered by the endocytic protein HIP1. *J. Neurosci.* 27, 2298–2308.
- Ming, G.-L., Song, H., 2011. Adult neurogenesis in the mammalian brain: significant answers and significant questions. *Neuron* 70, 687–702.
- Mira, H., Andreu, Z., Suh, H., Lie, D.C., Jessberger, S., Consiglio, A., San Emeterio, J., Hortiguera, R., Marques-Torres, M.A., Nakashima, K., Colak, D., Gotz, M., Fariñas, I., Gage, F.H., 2010. Signaling through BMPR-IA regulates quiescence and long-term activity of neural stem cells in the adult hippocampus. *Cell Stem Cell* 7, 78–89.
- Morshead, C.M., Reynolds, B.A., Craig, C.G., McBurney, M.W., Staines, W.A., Morassutti, D., Weiss, S., van der Kooy, D., 1994. Neural stem cells in the adult mammalian forebrain: a relatively quiescent subpopulation of subependymal cells. *Neuron* 13, 1071–1082.
- MuhChyi, C., Juliandi, B., Matsuda, T., Nakashima, K., 2013. Epigenetic regulation of neural stem cell fate during corticogenesis. *Int. J. Dev. Neurosci.* 31, 424–433.
- Muroa, N., Matsuda, T., Noguchi, H., Koseki, H., Namihira, M., Nakashima, K., 2014. Characterization of Np95 expression in mouse brain from embryo to adult: a novel marker for proliferating neural stem/precursor cells. *Neurogenesis* 1, 1–11.
- Namihira, M., Kohyama, J., Semi, K., Sanosaka, T., Deneen, B., Taga, T., Nakashima, K., 2009. Committed neuronal precursors confer astrocytic potential on residual neural precursor cells. *Dev. Cell* 16, 245–255.
- Namihira, M., Nakashima, K., 2013. Mechanisms of astrocytogenesis in the mammalian brain. *Curr. Opin. Neurobiol.* 23, 921–927.
- Okamoto, S., Li, Z., Ju, C., Scholzke, M.N., Mathews, E., Cui, J., Salvesen, G.S., Bossy-Wetzell, E., Lipton, S.A., 2002. Dominant-interfering forms of MEF2 generated by caspase cleavage contribute to NMDA-induced neuronal apoptosis. *Proc. Natl. Acad. Sci. U. S. A.* 99, 3974–3979.
- Rhee, K.D., Yu, J., Zhao, C.Y., Fan, G., Yang, X.J., 2012. Dnmt1-dependent DNA methylation is essential for photoreceptor terminal differentiation and retinal neuron survival. *Cell Death Dis.* 3, e427.
- Robertson, K.D., Wolffe, A.P., 2000. DNA methylation in health and disease. *Nat. Rev. Genet.* 1, 11–19.
- Sen, G.L., Reuter, J.A., Webster, D.E., Zhu, L., Khavari, P.A., 2010. DNMT1 maintains progenitor function in self-renewing somatic tissue. *Nature* 463, 563–567.
- Seri, B., Garcia-Verdugo, J.M., McEwen, B.S., Alvarez-Buylla, A., 2001. Astrocytes give rise to new neurons in the adult mammalian hippocampus. *J. Neurosci.* 21, 7153–7160.
- Sharif, J., Muto, M., Takebayashi, S., Suetake, I., Iwamatsu, A., Endo, T.A., Shinga, J., Mizutani-Koseki, Y., Toyoda, T., Okamura, K., Tajima, S., Mitsuya, K., Okano, M., Koseki, H., 2007. The SRA protein Np95 mediates epigenetic inheritance by recruiting DNMT1 to methylated DNA. *Nature* 450, 908–912.
- Simon, R., Brylka, H., Schwegler, H., Venkataramanappa, S., Andrantschke, J., Wiegrefe, C., Liu, P., Fuchs, E., Jenkins, N.A., Copeland, N.G., Birchmeier, C., Britsch, S., 2012. A dual function of Bcl11b/Ctip2 in hippocampal neurogenesis. *EMBO J.* 31, 2922–2936.
- Snyder, J.S., Choe, J.S., Clifford, M.A., Jeurling, S.I., Hurley, P., Brown, A., Kamhi, J.F., Cameron, H.A., 2009. Adult-born hippocampal neurons are more numerous, faster maturing, and more involved in behavior in rats than in mice. *J. Neurosci.* 29, 14484–14495.
- So, A.Y., Jung, J.W., Lee, S., Kim, H.S., Kang, K.S., 2011. DNA methyltransferase controls stem cell aging by regulating BMI1 and EZH2 through microRNAs. *PLoS ONE* 6, e19503.
- Steiner, B., Klempin, F., Wang, L., Kott, M., Kettenmann, H., Kempermann, G., 2006. Type-2 cells as link between glial and neuronal lineage in adult hippocampal neurogenesis. *Glia* 54, 805–814.
- Suzuki, M.M., Bird, A., 2008. DNA methylation landscapes: provocative insights from epigenomics. *Nat. Rev. Genet.* 9, 465–476.
- Takizawa, T., Nakashima, K., Namihira, M., Ochiai, W., Uemura, A., Yanagisawa, M., Fujita, N., Nakao, M., Taga, T., 2001. DNA methylation is a critical cell-intrinsic determinant of astrocyte differentiation in the fetal brain. *Dev. Cell* 1, 749–758.
- Temple, S., 2001. The development of neural stem cells. *Nature* 414, 112–117.
- Tsai, C.C., Su, P.F., Huang, Y.F., Yew, T.L., Hung, S.C., 2012. Oct4 and Nanog directly regulate Dnmt1 to maintain self-renewal and undifferentiated state in mesenchymal stem cells. *Mol. Cell* 47, 169–182.
- Zeron, M.M., Fernandes, H.B., Krebs, C., Shehadeh, J., Wellington, C.L., Leavitt, B.R., Baimbridge, K.G., Hayden, M.R., Raymond, L.A., 2004. Potentiation of NMDA receptor-mediated excitotoxicity linked with intrinsic apoptotic pathway in YAC transgenic mouse model of Huntington's disease. *Mol. Cell. Neurosci.* 25, 469–479.
- Zhou, Z., Hong, E.J., Cohen, S., Zhao, W.N., Ho, H.Y., Schmidt, L., Chen, W.G., Lin, Y., Savner, E., Griffith, E.C., Hu, L., Steen, J.A., Weitz, C.J., Greenberg, M.E., 2006. Brain-specific phosphorylation of MeCP2 regulates activity-dependent Bdnf transcription, dendritic growth, and spine maturation. *Neuron* 52, 255–269.
- Zhu, Y., Romero, M.I., Ghosh, P., Ye, Z., Charnay, P., Rushing, E.J., Marth, J.D., Parada, L.F., 2001. Ablation of NF1 function in neurons induces abnormal development of cerebral cortex and reactive gliosis in the brain. *Genes Dev.* 15, 859–876.



RESEARCH

Open Access

Differentiation of multipotent neural stem cells derived from Rett syndrome patients is biased toward the astrocytic lineage

Tomoko Andoh-Noda^{1,2}, Wado Akamatsu^{2,3*}, Kunio Miyake⁴, Takuya Matsumoto², Ryo Yamaguchi^{2,5}, Tsukasa Sanosaka², Yohei Okada^{2,6}, Tetsuro Kobayashi⁷, Manabu Ohyama⁷, Kinichi Nakashima⁸, Hiroshi Kurosawa¹, Takeo Kubota^{4*} and Hideyuki Okano^{2*}

Abstract

Background: Rett syndrome (RTT) is one of the most prevalent neurodevelopmental disorders in females, caused by *de novo* mutations in the X-linked methyl CpG-binding protein 2 gene, *MECP2*. Although abnormal regulation of neuronal genes due to mutant MeCP2 is thought to induce autistic behavior and impaired development in RTT patients, precise cellular mechanisms underlying the aberrant neural progression remain unclear.

Results: Two sets of isogenic pairs of either wild-type or mutant *MECP2*-expressing human induced pluripotent stem cell (hiPSC) lines were generated from a single pair of 10-year-old RTT-monozygotic (MZ) female twins. Mutant *MeCP2*-expressing hiPSC lines did not express detectable MeCP2 protein during any stage of differentiation. The lack of MeCP2 reflected altered gene expression patterns in differentiated neural cells rather than in undifferentiated hiPSCs, as assessed by microarray analysis. Furthermore, MeCP2 deficiency in the neural cell lineage increased astrocyte-specific differentiation from multipotent neural stem cells. Additionally, chromatin immunoprecipitation (ChIP) and bisulfite sequencing assays indicated that anomalous glial fibrillary acidic protein gene (*GFAP*) expression in the MeCP2-negative, differentiated neural cells resulted from the absence of MeCP2 binding to the *GFAP* gene.

Conclusions: An isogenic RTT-hiPSC model demonstrated that MeCP2 participates in the differentiation of neural cells. Moreover, MeCP2 deficiency triggers perturbation of astrocytic gene expression, yielding accelerated astrocyte formation from RTT-hiPSC-derived neural stem cells. These findings are likely to shed new light on astrocytic abnormalities in RTT, and suggest that astrocytes, which are required for neuronal homeostasis and function, might be a new target of RTT therapy.

Keywords: Rett syndrome, Methyl CpG-binding protein 2/MeCP2, Induced pluripotent stem cell, Neural stem cell, Astrocytes, DNA methylation

Background

Rett syndrome (RTT; MIM 312750) is a representative X-linked neurodevelopmental disease distinguished by repetitive and stereotypic hand movements replacing purposeful hand use, accompanied by gait ataxia, seizures, and autistic features. Patients present with apparently

normal psychomotor development during the first 6–18 months of life, followed by a short period of developmental stagnation, and then rapid disease progression with the characteristic features described above [1]. The incidence of RTT is 1 in 10,000–15,000 female births [2,3]. A linkage analysis demonstrated that the region harboring a causative gene is located between Xq27 and Xqter [4]. Meanwhile, a mutation analysis identified an X-linked gene encoding methyl-CpG-binding protein 2 (MeCP2) in the Xq28 region as the cause of RTT, where >~95% of patients with a classic RTT phenotype carry the *MECP2* mutation [5,6].

* Correspondence: awado@juntendo.ac.jp; takeot@yamanashi.ac.jp; hidokano@a2.keio.jp

²Department of Physiology, Keio University School of Medicine, 35 Shinanomachi, Shinjuku-ku, Tokyo 160-8582, Japan

⁴Department of Epigenetic Medicine, Faculty of Medicine, University of Yamanashi, 1110 Shimokato, Chuo, Yamanashi 409-3898, Japan

Full list of author information is available at the end of the article



MeCP2 is a transcription repressor that inhibits transcription by binding to methylated CpG dinucleotides, and also by recruiting co-repressors and chromatin remodeling proteins [7]. Thus, mutant MeCP2 affects large-scale chromatin organization [8], resulting in the mal-regulation of a number of genes, including neural and synaptic genes [9-13]. Furthermore, because RTT is an X-linked dominant disorder, phenotypic differences between female RTT patients have generally been attributed to variances in X chromosome inactivation (XCI) patterns, with skewing in favor of the mutant allele for the more severe clinical phenotypes [14-16].

Nevertheless, it remains unknown how developmental defects occur in the RTT brain at the cellular level. Recently, human induced pluripotent stem cell (hiPSC) technology has facilitated the modeling of neurological diseases by permitting the reprogramming of somatic cells into pluripotent cells [17]. So far, several studies have been performed with hiPSCs derived from patients with RTT and other neurological and neurodevelopmental diseases [18-26]. Previous reports of differentiated cells derived from RTT patient-specific hiPSCs demonstrated several abnormal *in vitro* phenotypes, such as diminished cell soma and nuclear sizes, reduced expression of neuronal markers, and attenuated dendritic spine density [19,21-24].

We recently reported a rare monozygotic (MZ) case of RTT in twins in which the genomic sequences were identical, including a *MECP2* frame-shift mutation (G269AfsX288) [27]. Interestingly, the patients (designated the RTT-MZ twins) showed divergent symptom severity regarding impaired neurological development, despite an identical genomic structure. Taking advantage of the nonrandom pattern of XCI in female hiPSCs [23] and the shared genetic background of the RTT-MZ twins [27], we aimed to generate two sets of isogenic pairs of wild-type *MECP2*- and mutant *MECP2*-expressing hiPSC lines from the RTT-MZ individuals. We then went on to show detailed defects in neural cells related to MeCP2 protein deficiency-induced developmental defects in RTT. Furthermore, we set out to clarify whether epigenetic and environmental cues participate in the abnormal neural development of RTT patients by comparison of the RTT-hiPSC lines derived from the RTT-MZ twin patients, who presented with varying symptom severity.

Results

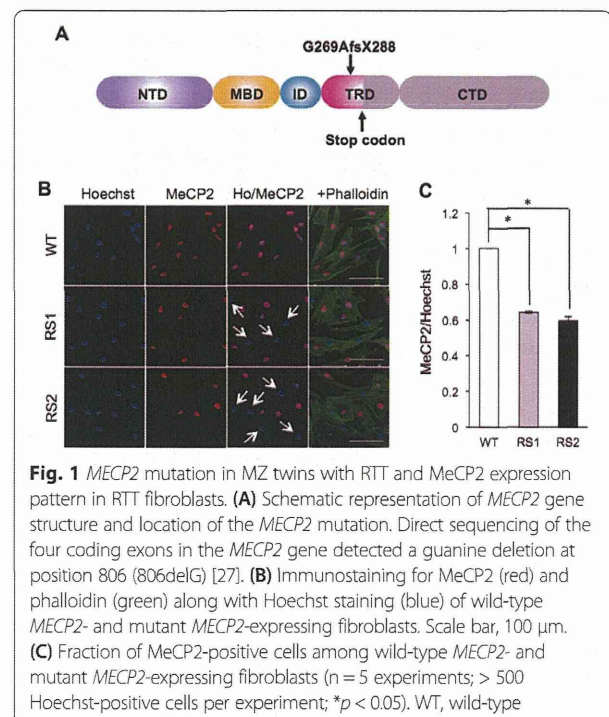
Mosaic expression patterns in fibroblasts procured from RTT-MZ twins

We recently established fibroblast cell lines from the RTT-MZ twins (patients RS1 and RS2). These RTT twins have a *de novo* frame-shift mutation in exon 4 (c.806delG) that truncates the MeCP2 protein within the

transcriptional repression domain (Fig. 1A). We also reported that fibroblasts generated from both patients exhibited random XCI patterns [27], which were detected by the methylation-specific polymerase chain reaction (PCR)-based HUMARA (human androgen receptor) XCI assay [28]. To examine the expression patterns of MeCP2 in RS1 and RS2 fibroblasts, immunostaining was performed with a specific primary antibody against MeCP2. Consequently, the fibroblast lines derived from the RTT-MZ twins included both MeCP2-positive and MeCP2-negative cells (Fig. 1B). Such mosaic expression patterns for the MeCP2 suggests that the fibroblasts comprise MeCP2-positive cells with the X chromosome harboring wild-type *MECP2* as the active MeCP2 species, and MeCP2-negative cells with the X chromosome harboring mutant *MECP2* as the active MeCP2 species. The fractions of MeCP2-positive cells among the RS1 and RS2 fibroblasts were 0.64 and 0.60, respectively (Fig. 1C).

Generation and characterization of RTT-MZ hiPSC lines

We utilized standard methods and transduction of *OCT4*-, *SOX2*-, *KLF4*-, and *c-MYC*-containing retroviruses to reprogram fibroblasts derived from the RTT-MZ twins into RTT-hiPSCs. Each RTT-hiPSC clone was clonally isolated and selected by morphological criteria and transgene silencing. We also verified pluripotency of the stem cells by immunostaining of the hiPSCs with primary antibodies against pluripotency markers (NANOG, OCT4, and TRA-1-81) (Fig. 2A and Additional file 1A).



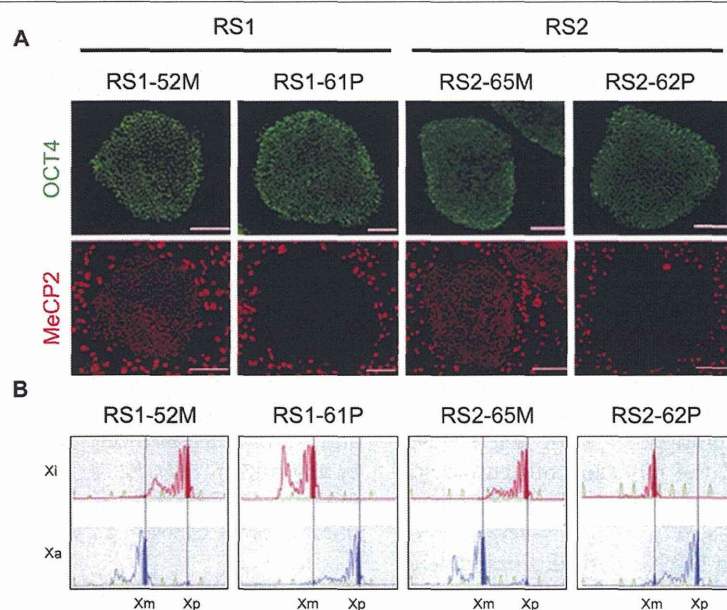


Fig. 2 hiPSC lines and XCI patterns derived from the RTT-MZ twins. **(A)** MeCP2 (red) and OCT4 (green) expression in hiPSC lines derived from the RTT-MZ twins. Scale bar, 150 μ m. **(B)** XCI patterns in the four hiPSC lines, as assessed by the methylation-specific PCR-based HUMARA assay. Xi, X inactivation pattern based on the inactive X chromosome; Xa, X inactivation pattern based on the active X chromosome; Xm, X chromosome inherited from the mother; Xp, X chromosome inherited from the father

To evaluate *in vivo* pluripotency, we injected the RTT-hiPSCs into the testes of immunodeficient mice, and confirmed the formation of teratomas containing derivatives of all three embryonic germ layers (Additional file 1B). No abnormalities were found in the karyotypes of any of the hiPSC lines (Additional file 1C). Notably, most of the selected hiPSC clones were either all MeCP2-positive or MeCP2-negative, and putatively originated from a single MeCP2-positive or MeCP2-negative fibroblast (Fig. 2A). Therefore, we isolated both wild-type *MECP2*-expressing (RS1-52 M and RS2-65 M) and mutant *MECP2*-expressing (RS1-61P and RS2-62P) clones from each patient (RS1 and RS2) to generate four hiPSC lines.

We next analyzed the XCI patterns in the hiPSC lines, and found that the maternal X chromosome was active in the MeCP2-positive (RS1-52 M and RS2-65 M) clones, while the paternal X chromosome was active in the MeCP2-negative (RS1-61P and RS2-62P) clones (Fig. 2B). Although we isolated several clones that partially include iPSC cells with two active X chromosomes, we only used clones with an inactive X chromosome (i.e., the “standard” XCI status of undifferentiated hiPSCs [29]) in the present study.

Our previous study [27] revealed that the maternally-derived X chromosome carries the wild-type *MECP2* allele, whereas the paternally-derived X chromosome carries the mutant *MECP2* allele. These results were

shown by sequencing the *MECP2* gene in somatic hybrid cell clones carrying either the maternal or the paternal X chromosome of the RTT-MZ twins. Accordingly, the RS1-52 M and RS2-65 M hiPSC lines, in which maternal wild-type *MECP2* was preferentially active, exhibited MeCP2 expression in the nuclei, whereas the RS1-61P and RS2-62P hiPSC lines, in which paternal mutant *MECP2* was preferentially active, did not (Fig. 2A).

MeCP2 expression in neural cells differentiated from RTT-hiPSCs

We next differentiated the four RTT-hiPSC lines into neural cells and examined MeCP2 expression in the progeny. Immunostaining revealed that all of the cells derived from the RS1-52 M and RS2-65 M hiPSC lines (containing preferentially active maternal wild-type *MECP2*) expressed MeCP2 in the nucleus, like the parental hiPSCs. In particular, MAP2-positive neurons expressed MeCP2 more strongly than glial fibrillary acidic protein (GFAP)-positive astrocytes (Fig. 3A) as previously shown in mice [30,31]. However, no MeCP2 expression was found in the progeny of the RS1-61P and RS2-62P hiPSC lines (containing preferentially active paternal mutant *MECP2*), or in the nucleus of RS1-61P/RS2-62P hiPSC-derived MAP2-positive neurons or GFAP-positive astrocytes (Fig. 3A). Therefore, neural cells differentiated from the RTT-hiPSC lines apparently retain the XCI status of the undifferentiated cells.

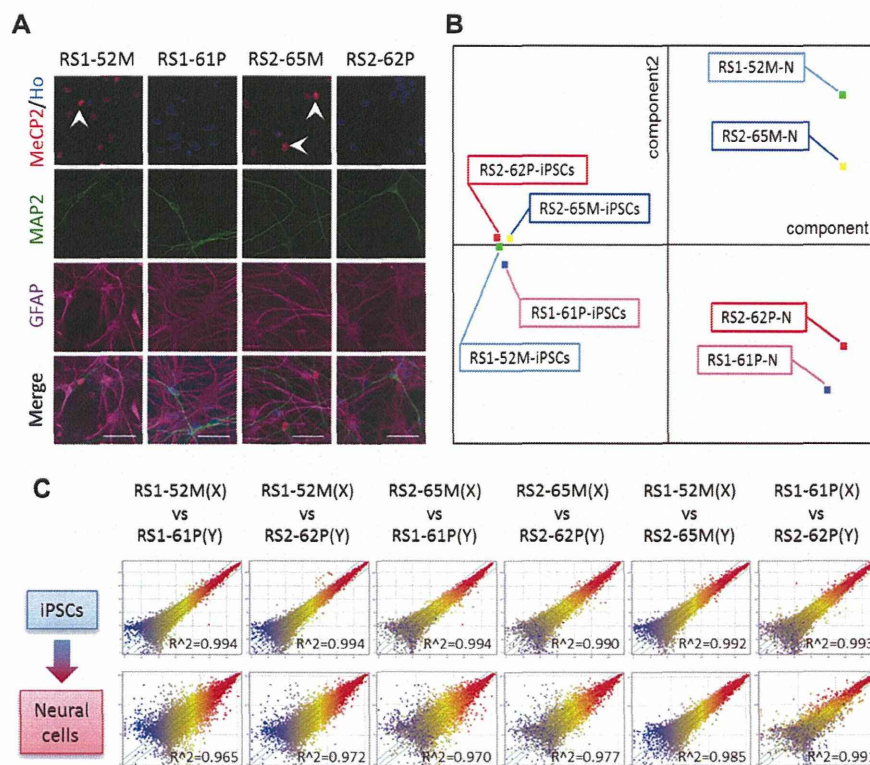


Fig. 3 Immunostaining of neural cells derived from RTT-hiPSCs and gene expression analysis of hiPSC-derived neural cells. **(A)** Immunostaining was performed to evaluate expression levels of MeCP2 (red), the neuronal marker, MAP2 (green), and the astrocytic marker, GFAP (magenta) in RTT-hiPSC-derived neural cells. Ho, Hoechst (blue). Arrowhead indicated MAP2, MeCP2 and Hoechst positive cells. Scale bar, 50 μ m. **(B)** Results of PCA (performed by using MeV software (TIGR) Software) of microarray gene expression in RTT-hiPSC lines and neural cells differentiated from RTT-hiPSC lines. N, neural cells differentiated from hiPSC lines. **(C)** Scatter plots of microarray gene expression in hiPSC-RTT lines and neural cells differentiated from hiPSC-RTT lines. Neural cells were co-cultured for ~30 days with mouse astrocytes

Global gene expression in RTT-hiPSCs and differentiated neural cells

We next investigated whether the loss of MeCP2 protein affects the transcriptional network in undifferentiated hiPSCs and neural progeny differentiated from RTT-hiPSCs. Global gene expression levels in wild-type *MECP2*- and mutant *MECP2*-expressing cells were examined by comparative microarray analyses of undifferentiated hiPSCs and differentiated neural cells. The gene expression data were normalized and subjected to principal component analysis (PCA) and hierarchical clustering, with the exception of those genes with low expression in all samples.

The samples were clustered into hiPSC or neural cell (N) groups depending on the *MECP2* expression pattern. In the PCA analysis, the original hiPSCs were clustered tightly into one region, signifying few differences from one hiPSC clone to the next. On the other hand, the neural cells were roughly clustered into two groups that reflected the status of the activated X chromosome (Fig. 3B and Additional file 2). Next, we constructed

scatter plots to compare wild-type *MECP2*- and mutant *MECP2*-expressing cells. In the undifferentiated hiPSCs, the correlation coefficient (R^2) was > 0.99 for any pair of hiPSC clones. However, in the differentiated neural cells, higher correlations ($R^2 > 0.98$) were only found in comparisons of hiPSCs with the same XCI pattern (i.e., paternal X vs. paternal X or maternal X vs. maternal X), while lower correlations ($R^2 < 0.98$) were only found in comparisons of hiPSCs with different XCI patterns (paternal X vs. maternal X) (Fig. 3C). The clustering dendrogram (Additional file 3A) also showed that global gene expressions for all four RTT-hiPSC clones during the undifferentiated stage. After this time, mutant *MECP2*-expressing hiPSCs became distinguishable from wild-type *MECP2*-expressing hiPSCs due to neural differentiation. Nevertheless, Tanaka et al. [25] recently characterized five patient-specific cell lines with different mutations to show that hiPSCs with *MECP2* gene mutations are distinguishable from normal hiPSCs and ESCs even during the undifferentiated stage. By contrast, our isogenic cell lines might largely exclude the effect of

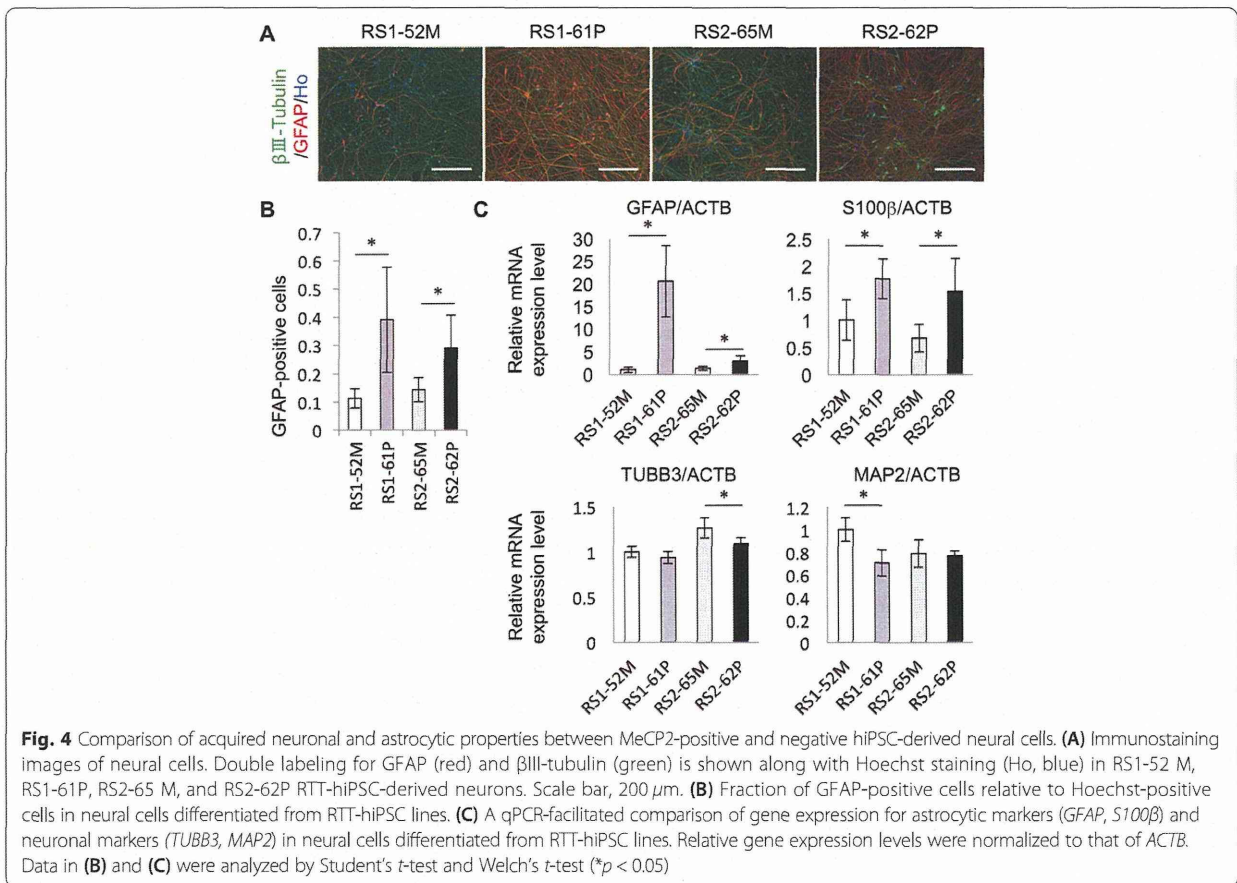
donor divergence, permitting the elucidation of *MECP2* function during neural differentiation. While Tanaka and colleagues [25] demonstrated that the gene expression of a key mitochondrial transcription factor, *NR3C1*, was upregulated in mutant *MECP2*-expressing cells after neuronal differentiation, we failed to detect such a difference in the current study (Additional file 3B). These results suggest that MeCP2 plays a more important role as a transcriptional regulator in differentiated neural cells than in undifferentiated hiPSCs.

Enhanced astrocytic differentiation of mutant *MECP2*-expressing neural stem cells derived from RTT-hiPSCs

Previous studies revealed that MeCP2 is involved in the regulation of astroglial gene expression [32-34]. *Gfap* and *S100β* are expressed at significantly higher levels in astrocytes derived from MeCP2-null mouse embryonic stem cells than in those derived from wild type mouse embryonic stem cells [35,36]. Moreover, a truncated form of RTT-associated MeCP2 (R168X) is reported to be unable to promote neuronal differentiation in mice, and instead promotes an abnormally high degree of astrocytic differentiation [37]. We characterized neurospheres derived from the four RTT-hiPSC lines (RS1-

61P, RS2-62P, RS1-52 M, and RS2-65 M), and found no significant differences in neurosphere number, size, or expression of neural stem cell markers between the two groups derived from mutant vs. wild-type *MECP2*-expressing hiPSCs (Additional file 4). Next, the neurospheres were differentiated into neural cells by using an adhesion culture method without fibroblast growth factor-2 (FGF-2) at ~30 days *in vitro* (Fig. 4A). The differentiated cells were classified by their expression of βIII-tubulin and GFAP. Immunocytochemical analysis revealed that the neural cells originating from MeCP2-negative hiPSC lines (RS1-61P and RS2-62P) contained significantly higher proportions of GFAP-positive cells than those originating from MeCP2-positive hiPSC lines (RS1-52 M and RS2-65 M) (Fig. 4B). Most of the GFAP-positive cells failed to express neuronal markers; therefore, we concluded that these cells were in fact astrocytes.

During the neural development of the mammalian central nervous system (CNS), neural stem cells initially differentiate into neurons, followed by astrocytes and oligodendrocytes at a later stage. We and others reported that MeCP2 binds to the promoter region of astrocyte-specific genes, including *S100β* and *Gfap*, to inhibit the conversion of neurons into astrocytes in



mammals [33,34,37-39]. To determine how MeCP2-regulated astrocyte-specific genes are influenced by the absence of MeCP2, we next examined the expression of *S100 β* and *GFAP* in MeCP2-negative and MeCP2-positive neural cells. As a result, MeCP2-negative RS1-61P and RS2-62P neural cells showed significantly enhanced expression of the astrocyte-specific genes, *GFAP* and *S100 β* (Fig. 4C). However, decreased expression levels of the neuronal genes, *TUBB3* and *MAP2*, were observed in several samples (i.e., *TUBB3* in RS2-62P cells and *MAP2* in RS1-61 cells) (Fig. 4C). These observations suggest that MeCP2 deficiency in the neural cell lineage increases astrocytic differentiation from multipotent neural stem cells.

Lack of MeCP2 binding to the *GFAP* gene in RTT-hiPSC-derived neural stem cells

MeCP2 was previously reported to bind to the highly methylated exon 1 region of the *Gfap* gene in mouse neurons [33,38]. To confirm these results in wild-type or mutant *MECP2*-expressing neurospheres, we performed chromatin immunoprecipitation (ChIP) assays with a specific primary antibody against MeCP2. Binding data were quantitated via real-time PCR by using primers spanning from the STAT3 binding site within the *GFAP* promoter to exon 1, relative to the transcription start site of *GFAP* (Fig. 5A, indicated by blue bidirectional arrows). For both the STAT3 binding site and *GFAP*

exon 1, precipitated genomic fragments were scarcely detectable by quantitative PCR (qPCR) in neurospheres derived from mutant *MECP2*-expressing hiPSC lines (RS1-61P, RS2-62P), while significant precipitation of genomic fragments was detected in neurospheres derived from wild-type *MECP2*-expressing hiPSC lines (RS1-52 M and RS2-65 M) (Fig. 5B).

Based on these results, we hypothesized that the increased expression of *GFAP* was induced by lack of direct MeCP2 binding to the *GFAP* gene in the mutant *MECP2*-expressing cells. However, it is possible that MeCP2 dysfunction indirectly enhanced the maturation of neural stem cells with truncated MeCP2, accompanied by decreased methylation of *gfap* [33], which might in turn modify MeCP2 protein recruitment. Thus, we performed bisulfite sequencing at the STAT3 binding site within the *GFAP* locus (Fig. 5A, indicated by black bidirectional arrows) by using wild-type or mutant *MECP2*-expressing neurospheres. Nevertheless, the MeCP2 binding sites in the *GFAP* gene were similarly hypermethylated in both wild-type and mutant *MECP2*-expressing neural stem cells differentiated from the four hiPSC lines (Fig. 5C). These findings signify that aberrant *GFAP* gene expression in neural stem cells containing truncated MeCP2 is not caused by changes in DNA methylation status (i.e., hypomethylation) within the genomic region encompassing the STAT3 binding site. Instead, the aberrant gene expression may be due to alterations in the amount of MeCP2 that

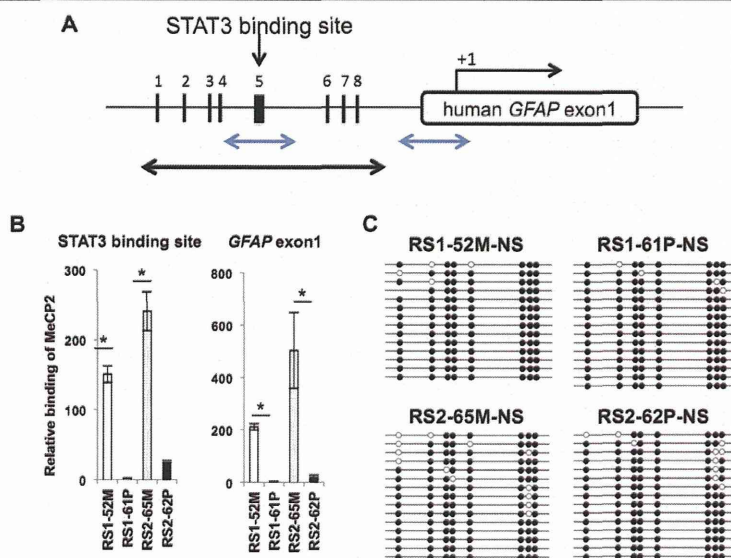


Fig. 5 MeCP2 binding analysis and DNA methylation status of the *GFAP* promoter region. **(A)** Schematic representation of the *hGFAP* genomic locus. ChIP/qPCR analysis was performed for the genomic regions (i.e., the STAT3 binding site and *GFAP* exon 1) indicated by the blue bidirectional arrows. Bisulfite sequencing was performed for the genomic region indicated by the black bidirectional arrows. **(B)** MeCP2 binding to the STAT3 binding site within the *GFAP* promoter region was quantified via ChIP/qPCR analysis by using an anti-MeCP2 antibody in neural cells differentiated from RTT-hiPSC lines. **(C)** Methylation frequencies of (1) the CpG site within the STAT3 recognition sequence and (2) seven other CpG sites around this sequence were analyzed in hiPSC-derived neurospheres via bisulfite sequencing

binds to the STAT3 binding site within the *GFAP* promoter and the *hGFAP* exon1.

Discussion

Female RTT patients display somatic mosaicism, because the *MECP2* gene is located on the X chromosome and undergoes random XCI. Here, we successfully generated two kinds of isogenic RTT-hiPSC lines that expressed only the wild-type or the mutant *MECP2* allele from the same RTT patient. So far, several groups have demonstrated disease modeling of RTT by using patient-specific hiPSCs [19,21-24]. However, some of these studies were conducted by comparisons between mutant hiPSCs derived from RTT patients and control hiPSCs derived from healthy subjects [19].

Regarding hiPSC technologies, clonal variations caused by donor differences and cell types of origin reportedly determine the differentiation potential of hiPSC clones. Hence, isogenic controls genetically engineered by using ZFN, TALEN or CRISPR-Cas9 systems are required for precise disease modeling with patient-specific hiPSCs [40]. Our isogenic RTT-hiPSC system has two significant advantages over these previous systems. First, our system allows clonal generation of hiPSCs expressing either wild-type or mutant MeCP2 protein. Second, the generated hiPSCs are isogenic without genetic engineering. By utilizing our homogenous RTT-hiPSC populations, we were able to show that global gene expression patterns were distinctly different between wild-type MeCP2-cells and mutant MeCP2-expressing cells in terms of both neurospheres and differentiated neural stem cells. Although MeCP2 was weakly expressed in undifferentiated wild-type hiPSCs, significant differences in gene expression profiles were not observed among the four hiPSC lines. These results suggest that the MeCP2 primarily functions in cells already committed to a neural lineage.

We also found increased proportions of astrocytes among mutant MeCP2-expressing neural cells compared with wild-type MeCP2-expressing neural cells. Other investigators similarly documented MeCP2 expression in glial cells, including astrocytes [41], implying that glial MeCP2 might play a distinct role in the maintenance of neuronal functions, such as neuronal maturation and/or dendritic arborization [42]. Although previous studies showed that a conditional MeCP2 knockout mouse (which lacked MeCP2 expression in mature neurons) displayed a RTT-like neurological phenotype, mutant astrocytes derived from this model mouse failed to support normal dendritic arborization of either wild-type or mutant neurons [30]. Furthermore, mutant *MECP2*-expressing astrocytes differentiated from RTT-hiPSCs apparently had significant effects on wild-type neurons [26]. Intriguingly, another study in mice showed that the MeCP2-deficient state can spread between astrocytes via gap junctions [43].

The current investigation did not examine dendritic phenotypes in neurons derived from RTT-hiPSCs. However, our model may be useful for mixed culture experiments (i.e., wild-type *MECP2*-expressing neurons and mutant *MECP2*-expressing astrocytes) to distinguish cell-autonomous from non-cell-autonomous effects in RTT patient-derived neural cells. Additionally, we demonstrated that astrocytic marker genes, particularly *GFAP*, were aberrantly expressed under conditions of MeCP2 deficiency due to the deregulation of transcription, and we employed CHIP and bisulfite sequencing analyses to show induction of *GFAP* expression in RTT-hiPSC-derived neural cells caused by the absence of direct binding of mutant MeCP2 to the *GFAP* gene. Hence, mutant MeCP2 may contribute to the excessive differentiation of *GFAP*-positive astrocytes.

Several groups reported that human female RTT patients present with microcephalic brains, as do male and female Rett syndrome model mice [44-46]. Moreover, analysis of postmortem brain tissue from RTT patients revealed increased *GFAP* protein expression in the RTT brain [32]. Consistent with these results, we anticipate that the brains of RTT patients will exhibit a larger than normal percentage of astrocytes. Thus, astrocytes differentiated from RTT patient-derived, mutant *MECP2*-expressing hiPSC lines may be useful for drug development for RTT therapy, because some drugs for mental disorders (e.g., antidepressants) affect not only neurons, but also activate astrocytes. The activated astrocytes then go on to carry out specific functions that result in the reactivation of cortical plasticity, potentially leading to the readjustment of abnormal neural networks [47,48].

This study aimed to clarify the involvement of epigenetic and environmental cues in the neural development of RTT-MZ twins (patients RS1 and RS2) with differing symptom severity. Although we successfully generated hiPSCs from both patients, no significant differences in mutant MeCP2 phenotypes were observed between RS1 and RS2 cells. These results suggest that epigenetic and environmental cues might work together to affect the neural phenotypes of RTT patients. Another possibility is that skewed XCI occurs in the CNS in RTT patients. Although we previously reported that biased XCI does not take place in the other somatic cells (i.e., skin, blood, and hair) of these patients [27], biased XCI in the CNS may underlie the discrepancy in symptom severity between isogenic RTT-MZ twin patients.

Conclusions

In summary, we successfully generated two sets of isogenic RTT-hiPSC lines that expressed only the wild-type or the mutant *MECP2* allele from the same RTT patient, and revealed that abnormal astrocytic differentiation is involved in RTT pathogenesis. Specifically, we used hiPSC

technology to show that (1) MeCP2 protein deficiency results in dysregulation of *GFAP* expression in mutant *MECP2*-expressing neural cells, and (2) an increased number of astrocytes are differentiated from RTT-hiPSC-derived neural stem cells carrying mutant vs. wild-type *MECP2*.

Materials and methods

Isolation of skin fibroblasts and generation of hiPSCs

A skin-punch biopsy from a single pair of 10-year-old Japanese MZ twins with RTT (patients RS1 and RS2) [27] was performed with written informed consent from their parents. The obtained fibroblasts were used to establish the four hiPSC lines discussed above. The study protocol was reviewed and approved by the Research Ethics Committees of Keio University (Approval No. 20080016) and the University of Yamanashi (Approval Nos. 523 and 699). This study was conducted in accordance with the principles expressed in the Declaration of Helsinki.

A standard retrovirus method was used to establish the hiPSCs. The maintenance of fibroblasts, lentiviral production, retroviral production, infection, stem cell culture, and characterization of hiPSCs was conducted as described previously [17].

Sample collection and DNA isolation

All peripheral blood, skin fibroblasts, and hiPSC samples used in this study were obtained from RTT-MZ patients whose parents gave informed consent for medical research at the University of Yamanashi and Keio University Hospital. DNA from lymphocytes, skin fibroblasts, and hiPSCs was extracted with the DNeasy Blood and Tissue Kit (QIAGEN) according to the manufacturer's instructions.

XCI analysis

XCI patterns were obtained in the extracted DNA by using a methylation-specific PCR-based method. Bisulfite treatment of genomic DNA followed by PCR was performed as previously described [28]. Briefly, DNA was treated with sodium bisulfite, and the treated DNA was amplified via PCR by using two primer sets (one for the methylated inactive X chromosome, and the other for the unmethylated active X chromosome). The primer sets were designed within the CpG island (exon 1) of the HUMARA gene located at Xq11-a12. The PCR products were mixed with a size standard and separated on an ABI 310 DNA Sequencer equipped with Genescan Software (Applied Biosystems).

Teratoma assay

Teratoma formation was assessed by injecting hiPSCs into the testes of 8-week-old NOD.CB17-*Prkdc*^{scid}/J mice

(OYC International, Inc.), as previously described [49]. Eight weeks after hiPSC transplantation, tumors were dissected and fixed with phosphate buffered saline (PBS) containing 4% formaldehyde. Paraffin-embedded tissue was sectioned and stained with hematoxylin & eosin. Images were obtained by using a BZ-9000 microscope (Keyence).

Karyotyping of hiPSCs

Standard G-banding analysis was performed in the four hiPSC lines (RS1-52 M, RS1-61P, RS2-65 M, and RS2-62P) to rule out the possibility of abnormal karyotypes that can occur during the generation of hiPSCs.

In vitro differentiation of hiPSCs

Neural differentiation of hiPSCs was performed as described previously [50], except that epidermal growth factor and Noggin were omitted from the culture system (Matsumoto et al., manuscript in submission). The hiPSCs were plated onto the bottom of T75 flasks (Nunc) and maintained for 14 days. Neurospheres were repeatedly passaged by dissociation into single cells, followed by culture in the same manner. Neurospheres were differentiated into neural cells by using an adhesion culture method without FGF-2, and then subjected to qPCR and immunostaining analysis. Typically, neurospheres between passages 3 and 10 were used for the analysis. RNA samples were collected on day 14 of neurosphere culture from an arbitrary number of cells. For terminal differentiation, neurospheres were cultured in 1 × B27 medium, dissociated neural precursor cells allowed to adhere to poly-L-ornithine-/fibronectin-coated coverslips and then cultured for 30–32 days. RNA was then isolated from terminally differentiated neurospheres. Alternatively, the differentiated cells were immunostained with primary antibodies against β III-tubulin and GFAP. Approximately 1×10^5 neural stem cells were plated onto 14-mm glass coverslips for immunostaining of differentiated neural cells, and $\sim 1.2 \times 10^6$ neural stem cells were plated onto a well using 6-well plate for RNA isolation from differentiated neural cells. For long-term neural differentiation, mouse astrocytes obtained from E16.5 ICR mice were utilized with a cell culture insert system (Falcon® product #353102). RNA samples were obtained from iPSCs, neurospheres, and neuronal cells at passages 12–20, passages 3–9 (day 14), and day 30–32, respectively.

Immunocytochemical analysis of hiPSCs and neural cells differentiated from hiPSCs

Cells were fixed with PBS containing 4% paraformaldehyde for 30 min at room temperature and incubated with primary antibodies against the following proteins: MeCP2 (1:200, Cell Signaling Technology), phalloidin

(1:2000, Dyomics), NANOG (1:500, CosmoBio), OCT4 (1:200, Santa Cruz Biotechnology, Inc.), TRA-1-60 (1:1000, Millipore), TRA-1-81 (1:1000, Millipore), β III-tubulin (1:2000, Sigma Chemical Co.), MAP2 (1:250, Sigma Chemical Co.), and GFAP (1:1000, Invitrogen). They were then washed with PBS and incubated with an Alexa Fluor 488-, Alexa Fluor 555-, or Alexa Fluor 647-conjugated secondary antibody (1:500, Invitrogen), as appropriate. Images were obtained using an Axioplan 2 microscope (Carl Zeiss). The number of GFAP-positive cells was counted among 100 Hoechst-positive cells for each experiment ($n = 5$).

Microarray analysis

For microarray analysis, RNA quality was assessed by using a 2100 Bioanalyzer (Agilent Technologies). Total RNA (100 ng) was reverse transcribed, biotin-labeled, and hybridized to a GeneChip[®] Human Genome U133 plus 2.0 Array (Affymetrix). The array was subsequently washed and stained in a Fluidics Station 450 (Affymetrix), as instructed by the manufacturer. The microarrays were scanned by using a GeneChip[®] Scanner 3000 (Affymetrix), and the raw image files were converted into normalized signal intensity values by using the MAS 5.0 algorithm.

Next, targets were selected that (a) were “present” in at least one of the eight arrays analyzed, and (b) had a probe intensity of ≥ 50 . In total, 23,463 targets were identified from this initial screen. The normalized logs were hierarchically clustered based on uncentered correlation with complete linkage by using Cluster 3.0 Software [51]. The PCA plot was generated by using TIGR MeV (Multiple Experimental Viewer) Software [52]. The three-dimensional image of the PCA plot and the scatter plot were generated by using GeneSpring GX Software (ver. 12.6.1).

Quantitative reverse transcription PCR (qPCR) assay

Total cellular RNA was extracted by using the TRIzol Reagent[®] (Life Technologies), the RNase-Free DNase Set (QIAGEN), and the RNeasy[®] Mini Kit (QIAGEN). Next, cDNA synthesis was performed by using the SuperScript III First-Strand Synthesis System for RT-PCR (Life Technologies) with oligo-dT primers according to the manufacturer’s guidelines. Real-time RT-PCR was then performed on a ABI PRISM[®] 7900HT Sequence Detection System (Applied BioSystems) by using SYBR Premix ExTaq[™] Tli RNaseH Plus (Takara). The qPCR amplification was performed by using the following primers: *GFAP*-forward (5'-TGTGAGGCAGAAGCTCCAGGATG A-3') and *GFAP*-reverse (5'-AGGGTGGCTTCATCTGCTTCCTGT-3'); *S100 β* -forward (5'-GTGGCCCTCATCGACGTTTT-3') and *S100 β* -reverse (5'-ACCTCCTGCTCTTGATTTCTCT-3'); *TUBB3*-forward (5'-ATTTTCATCT

TTGGTCAGAGTGGGGC-3') and *TUBB3*-reverse (5'-TGCAGGCAGTCGCAGTTTTTTCAC-3'); *MAP2*-forward (5'-GGCCCAAGCTAAAGTTGGTTCTC-3') and *MAP2*-reverse (5'-GCAGTGACATCCTCAGCCAAAG-3'); and *ACTB*-forward (5'-TGAAGTGTGACGTGGACATC-3') and *ACTB*-reverse (5'-GGAGGAGCAATGATCTTGAT-3'). Relative gene expression levels of *GFAP*, *S100 β* , *TUBB3*, and *MAP2* were normalized to *ACTB* expression and standardized by the RS1-52 M value, which was set to 1.

ChIP assay

Nuclei were obtained from neurospheres derived from each hiPSC line. ChIP was performed with antibodies against MeCP2 (Cell Signaling Technology), as described previously [53], with the following modifications. Neurospheres were crosslinked with 1% formaldehyde for 10 min to yield crosslinked chromatin. They were then incubated with glycine at a final concentration of 200 mM for another 5 min, and stored at -80°C until use. The lysed nuclear pellets were sonicated six times with a 30-sec ON, 60-sec OFF cycle by using a Bioruptor[®] Sonicator (Diagenode, Inc.). The crosslinked chromatin was subsequently eluted from magnetic beads (Dynabeads[®] M-280 Sheep anti-Rabbit IgG; Life Technologies). Co-immunoprecipitated DNA was detected via qPCR by using the following primers: STAT3 binding site-forward (5'-TCATGCCCAGTGAATGACTC-3') and STAT3 binding site-reverse (5'-AGATGCCAGGCTGTCAGG-3'); and *hGFAP* exon1-forward (5'-AGAGCAGGATGGAGAGGA GA-3') and *hGFAP* exon1-reverse (5'-CCTTGAAGCC AGCATTGAGT-3').

Bisulfite sequencing analysis

Sodium bisulfite treatment of genomic DNA was performed by using the Methylamp DNA Modification Kit (Epigentek) according to the manufacturer’s instructions. A region in the *GFAP* promoter region containing the STAT3 binding site was amplified from bisulfite-treated genomic DNA via PCR with the following forward and reverse primers: *hGFAP* promoter-forward (5'-TTGGGGAGGAG GTAGATAGTTAGGTTTT-3') and *hGFAP* promoter-reverse (5'-CATCCCCTAATCCCCTTTTCTTCTAAA-3'). PCR products were cloned into the pT7Blue vector (Novagen), and at least 12 randomly selected clones were sequenced.

Statistical analysis

All quantifiable data are expressed as the means \pm the standard deviation of the mean. The statistical significance of differences between conditions was analyzed by using Student’s *t*-test and Welch’s *t*-test. In all cases, *p* values of < 0.05 were considered statistically significant.